Environ Fluid Mech (2014) 14:771–794
DOI 10.1007/s10652-013-9323-2

ORIGINAL ARTICLE

Turbulence suppression by suspended sediment within a geophysical flow

Sean J. Bennett · Yinting Hou · Joseph F. Atkinson

Received: 31 January 2013 / Accepted: 5 November 2013 / Published online: 17 November 2013

Abstract Experiments are performed in a mixing box to evaluate the effect of suspended sediment on turbulence generated by an oscillating grid. Quartz-density sand of varying sizes and concentrations is used, and particle image velocimetry is employed to quantify only the fluid phase. Results show that (1) while a relatively large secondary flow field is present in the box, turbulence is a maximum near the grid and it decreases systematically toward the water surface; (2) relatively high concentrations of fine sediment can markedly alter this secondary flow field and significantly decrease both the time-mean and turbulent kinetic energy within the flow, yet these same sediment concentrations have little effect on the integral time and length scales derived for each velocity component; and (3) the overall turbulence suppression observed can be related to the transfer of energy from the fluid to the sediment and the maintenance of a suspended sediment load rather than commonly employed turbulence modulation criteria. These experimental data demonstrate unequivocally that the presence of a suspended sediment load can significantly reduce overall turbulent kinetic energy, and these results should be applicable to a range of sediment-laden geophysical flows.

Keywords Turbulence modulation · Mixing box · Particle image velocimetry · Sediment suspension

1 Introduction

Geophysical flows that entrain and transport sediment have been studied extensively and described analytically in a wide range of field, experimental, and engineering settings. Fundamental to the process of sediment transport is the transfer of fluid momentum from the

S. J. Bennett (✉)
Department of Geography, University at Buffalo, Buffalo, NY 14261-0055, USA
e-mail: seanb@buffalo.edu

Y. Hou · J. F. Atkinson
Department of Civil, Structural, and Environmental Engineering,
University at Buffalo, Buffalo, NY 14260, USA

carrier fluid to the sediment so that entrainment and transport can proceed [4,7,13]. Because of this fluid-particle interaction, it might be concluded that the hydrodynamic characteristics of the fluid phase would be measurably affected by this sediment transport process, either by enhancing (increasing) or suppressing (decreasing) fluid turbulence at a variety of time and length scales. There is ample experimental evidence to support the modulation of fluid turbulence by sediment in geophysical flows, displaying both behaviors under varying conditions (e.g., [14,15]).

A number of mechanisms have been proposed for the observed modulation of fluid turbulence by the presence of sediment. For dilute suspensions in geophysical and multiphase flows (e.g., gases, jets, open channels), turbulence reduction or suppression has been linked to the enhanced inertia and effective viscosity of the particle-laden flow, and the increased dissipation arising from particle drag [2]. Conversely, turbulence enhancement has been linked to higher velocity fluctuations due to wake dynamics and vortex shedding, and buoyancy-induced instabilities due to density variation arising from preferential particle concentration [2].

Much of the debate on turbulence modulation in open channel flow has focused on the mixing length concept. Several studies have examined how parameters such as turbulence intensity, von Kármán's coefficient, mixing length, and eddy viscosity are altered in the presence of a suspended sediment load (see reviews in [6,30]). For example, Best et al. [6] noted that, upon the addition of sediment to a clear-water flow, the mixing length and von Kármán coefficient can decrease, roughness height can increase, and turbulence intensities can increase near the bed and decrease higher in the flow. Nezu and Azuma [31] found that the von Kármán coefficient remains about the same, but turbulence intensities can be enhanced in the near-wall regions and show negligible modulation higher in the flow. Muste et al. [30] noted that the mixing length and von Kármán coefficient can decrease, turbulence intensities can increase in the near-wall regions, and turbulence intensities can display little to no change higher in the flow. Lyn [25,26] noted a similar increase in flow resistance due to the addition of suspended sediment, but the effect on turbulence characteristics was modest or negligible. It would appear that the overall effect of adding sediment to a clear-water open channel flow is to increase flow resistance, increase near-bed turbulence intensities, and alter mixing lengths.

Particle inertia often has been used to explain much of the turbulence modulation observed in open channel flows, and three parameters have been used to define and characterize these effects. The first criterion is based on particle diameter D, and suggests that when D is much smaller than the most energetic eddy, taken here as the integral length scale of turbulence λ, then the particle will follow the eddy for part of its transit time [14]. As such, a portion of the turbulent energy of the eddy is transformed into the kinetic energy of the particle (via a drag force), which reduces the turbulent energy of the fluid. When D is relatively larger, particles will tend to create turbulence in their wakes near the scale of the most energetic eddy λ, and increase the total turbulent energy of the fluid. The critical threshold for the transition from turbulence suppression to turbulence enhancement occurs at $D/\lambda = 0.1$ [14]. The second criterion suggests that turbulence modulation by suspended sediment occurs because a slip velocity exists between the particle in transport and the carrier fluid, which along with D can be used to define a particle Reynolds number Re_p. According to Hetsroni [16], when Re_p is relatively low, turbulence tends to be reduced in the presence of suspended sediment. Yet when Re_p is relatively high, particles in transport will shed vortices, and this phenomenon tends to increase fluid turbulence. Zhao et al. [39] further elaborated this criterion and suggested that since a slip velocity exists between the two phases, there is greater energy transfer from the fluid to the suspended sediment than vice versa, which results in a reduction of kinetic energy within the fluid. The third criterion suggests that turbulence modulation by suspended

sediment occurs because there is a difference in the response times of the particle in transport t_p and the carrier fluid t_f, and the ratio of these times defines the Stokes number St,

$$St = \frac{t_p}{t_f} = \frac{\frac{1}{18\nu} D^2 \frac{\sigma}{\rho}}{\lambda / u_{rms}} \tag{1}$$

where ν is kinematic viscosity, σ is particle density, ρ is fluid density, and u_{rms} is the root-mean-square of the primary flow velocity component (see below; [12,21]). According to Elghobashi [11], when St is relatively small, the surface area of the particles increases for a given volumetric suspended sediment concentration, which causes the rate of turbulence dissipation ε to increase. Whereas when St is relatively large, Re_p increases, which leads to vortex shedding and turbulence enhancement. This criterion has been criticized by Tanaka and Eaton [36] who proposed a new parameter to discriminate turbulence modulation that included both St and Re_p. This new criterion was shown to work well in gas flows modulated by particles. In addition, Lucci et al. [24] suggested that Eq. (1) should not be used to assess turbulence modulation by relatively large particles, or when the particle grain size D is about the same size as the Taylor turbulence length scale λ. This is because particle concentration at constant St could have different effects on turbulence.

The application of such criteria to the modulation of turbulence by sediment in open channel flows has not been fully successful. Both Best et al. [6] and Muste et al. [30] applied these criteria to explain their experimental observations. These experimental results include the following: (1) subtle, or negligible, rather than marked variations in velocity and turbulence signatures; (2) both enhancement and suppression of fluid turbulence at different locations in the same flow; (3) inconsistency in the effects of sediment on turbulent flow; and (4) the recognition that these criteria may not effectively capture or explain, in mechanistic terms, the occurrence of turbulence modulation.

The ambiguities of turbulence modulation encountered in open channel flows could be related to limitations in the experimental design and analytic framework. Given obvious experimental uncertainties, the very addition of sediment to a clear-water flow should be met with some measurable hydrodynamic adjustment, tempered by sediment size, density, and concentration. It is contended here that the experimental design to examine the effects of suspended sediment on fluid turbulence can be improved significantly by clearly and unambiguously discriminating between the fluid and sediment phases within a sediment-laden turbulent flow, and by ensuring that the clear-water and sediment-laden flows are hydrodynamically equivalent. Moreover, there has been an overreliance on empirically-derived expressions to assess turbulence modulation criteria (integral time and length scales for both particles and fluid), rather than deriving these critical parameters directly from the data collected.

The current research program is designed to address these limitations. First, particle image velocimetry (PIV) is employed to quantify the turbulent flow field, where laser-induced fluorescent tracer particles coupled with lens-mounted polarized filters ensure that only the characteristics of the fluid phase are captured. Second, a standard grid-mixing box is used (e.g., [38]), where the oscillation frequency and stroke of the grid are externally controlled and total flow depth is maintained with great precision. While an oscillating grid in a mixing box is, by definition, a zero mean-shear flow, the diffusion of fluid turbulence from the grid, and the dissipation of this energy, both are analogous to a wide range of geophysical flows including open channels (e.g., [18,20,28]). Third, all integral time and length scales of the sediment-laden flow used in the assessment of turbulence modulation criteria are derived directly from the data.

The overall goals of this research are to examine systematically the dynamics of sediment-laden geophysical flows in controlled laboratory conditions and to document the occurrence and hydrodynamic characteristics of turbulence modulation by sediment in transport. The objectives of the current paper are: (1) to quantify the time-mean and turbulent flow field within a zero-mean shear flow in the presence of suspended sediment of varying size and concentration; (2) to document and describe the hydrodynamic response of the turbulent flow to these suspended sediment loadings; and (3) to assess mechanisms of turbulence modulation within this sediment-laden geophysical flow. It is shown that suspended sediment, even in rather dilute concentrations, can markedly alter fluid turbulence, and its overall effect is to suppress the magnitude of these turbulent signatures. Companion and preliminary results from this experimental program are summarized in Bennett et al. [5]. The current paper expands greatly the experimental database assembled and the depth and breadth of the data analysis presented and discussed in that previous work.

2 Experimental equipment and procedure

2.1 Experimental setup

All experiments are performed in a polycarbonate mixing box 0.315 m wide and deep, and 0.393 m tall (Fig. 1). An oscillating aluminum grid placed at the bottom of the box provides the source of turbulence. This grid consists of ten 10-mm square bars with 50-mm center-to-center spacing (mesh spacing M of 40 mm), and it is mounted from above to a rotating eccentric arm and controlled by an external motor. The stroke of the grid S is 90 mm with its lowest position just above the floor of the box, and the speed of the motor, thus the oscillation frequency f of the grid, is measured with an optical tachometer. For all experiments, the box is filled with tap water to a depth of 0.29 m and a single oscillation frequency is used ($f = 2.33$ Hz). Flow and sediment data are presented as a function of height y above the apogee of the grid (where $y = 0$) and total flow depth d (maximum value of y) is 0.2 m.

Particle image velocimetry (PIV) is used to quantify all turbulence parameters within the box. This system comprises a dual-cavity 50 mJ Nd-YAG laser emitting 532 nm light and

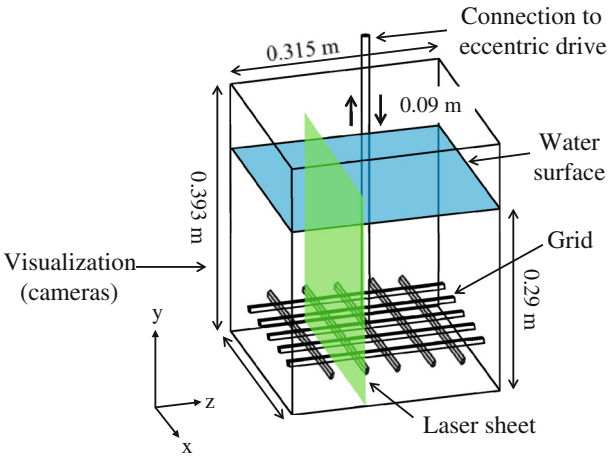

Fig. 1 Sketch of the mixing box showing all dimensions, the grid, and the position of the laser and cameras

two 4 Mp cameras each with 4 GB of RAM. All data acquisition and synchronization are handled by an external timing hub, dedicated computer, and commercial software. Inside the box at the apogee of the grid, a dual-level 3D calibration target (0.27 m wide and 0.19 m tall) is placed, and the cameras are mounted off-axis to the target (total angular difference of 16°). The measurement domain extends horizontally (x-direction) from $x/B = 0.08$ to $x/B = 0.92$, where B is the internal width of the box, and vertically (y-direction) from $y/d = 0.02$ to $y/d = 0.98$. The laser light sheet enters the box at 91 mm from the sidewall, and it is centered on the cross-bars of the grid rather than the nodes. Hollow glass spheres 20 to 50 μm in diameter and dyed with Rhodamine B are used as fluid tracer particles, which fluoresce in the laser light sheet. Polarizing filters (>570 nm) are placed on the camera lenses, thereby allowing only these fluorescent tracer particles to be recorded to video. Paired images are collected at 80 Hz, the interrogation areas are 32 pixels (ca. 4 × 4 mm), the time-interval between successive laser images is 2,800 μs, and the central-difference adaptive correlation algorithm within the commercial software is used to derive the 3D vector fields. Each data field comprises approximately 2,800 vectors, and about 450 image pairs are used to derive time-averaged values of mean and turbulent velocities in three directions ($u-$, $v-$, and w-components in the $x-$, y-, and z-directions, respectively), which spans about 13 grid oscillations. All data reported here are actual measurements, and all time-averaged values have a minimum of 100 validated signals.

Quartz-density sand of varying grain size and concentration is added to this box using these clear-water conditions. Five well-sorted sands, having a density σ of 2,650 kg/m^3, are used: 0.15–0.20, 0.25–0.30, 0.35–0.40, 0.7–0.8, and 1.0–1.2 mm in diameter. For each sand, total added mass to the box varies from 100–1,000 g at 100-g intervals, which is equivalent to a volumetric sediment concentration C_0 ranging from 0.0013 to 0.0130. Volumetric suspended sediment concentrations C are collected for select experiments at-a-point along the box centerline and as a function of y/d using a siphon sampler. Both the volume of water and sediment removed after each sample extraction are replaced by an equivalent amount. The water from these samples is decanted, and the sediment is oven-dried to determine volumetric concentration.

3 Results

3.1 Time-mean and turbulent flow using clear-water conditions

While the mixing box has no mean flow, oscillation of the grid creates a secondary circulation pattern present in all experiments. The time-mean 2D vectors (u- and v-components; w-component not shown here) and select streamlines for the clear-water conditions are shown in Fig. 2. It is well-known that an oscillating grid generates quasi-steady jet flow very close to each grid bar [38]. Above the grid, these jets interact and break down to create diffusing turbulence, whose magnitude decays with distance from the grid, as further modulated by the grid mesh spacing, oscillation frequency, and stroke [18]. For these experiments, flow within this plane of the mixing box is characterized by two large convection cells, and the largest magnitude secondary flow velocities are located in the center of the field and are vertically oriented. Two counter-rotating convection cells bound this central flow region, returning fluid to the bottom of the tank along the box sidewalls. Secondary circulation within mixing boxes already has been noted [10,28], and the secondary circulation pattern and magnitude observed here is a function of the boundary conditions imposed and the placement of the grid near the bottom of the box.

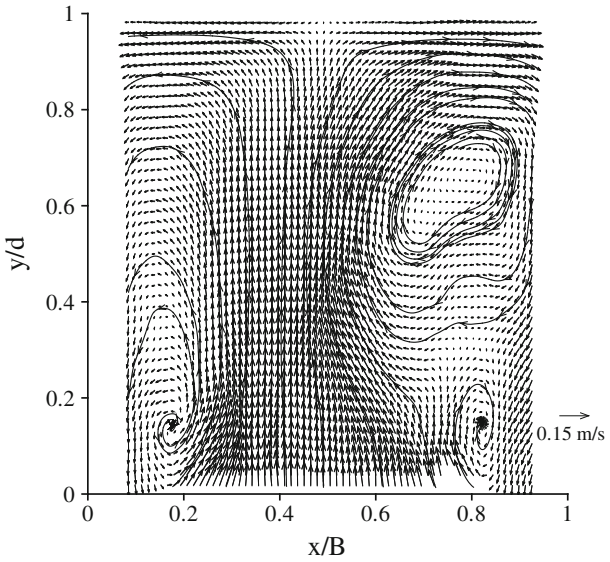

Fig. 2 Time-averaged 2D flow vectors and select streamlines within the mixing box for clear water conditions using $f = 2.33$ Hz

Turbulence parameters for the clear-water flow conditions can be defined based on previous work with mixing boxes. The magnitude of turbulence within a mixing box with square bars can be approximated by

$$\sqrt{\overline{u'^2}} = c_1 f S^{1.5} M^{0.5} y^{-1}; \quad \sqrt{\overline{v'^2}} = c_2 f S^{1.5} M^{0.5} y^{-1}; \quad k = c_3 f^2 S^3 M y^{-2} \tag{2}$$

where the root-mean-square velocities are defined as $u_{rms} = \sqrt{\overline{u'^2}}$ and $v_{rms} = \sqrt{\overline{v'^2}}$, $u' = u - \bar{u}$, $v' = v - \bar{v}$, and $w' = w - \bar{w}$, with the overbar signifying a time-averaged value and the prime indicating a time-fluctuating value, turbulent kinetic energy is defined as $k = 0.5\left(\overline{u'^2} + \overline{v'^2} + \overline{w'^2}\right)$, and c_1, c_2, and c_3 are constants [8,18,33]. For a given f, S, and M, the magnitude of the secondary turbulent velocities should decrease linearly with distance from the grid, whereas turbulent kinetic energy should decrease with the square of this distance. In a companion study, contour maps of these turbulence parameters showed that higher magnitude values in the mixing box were in close association with distance from the grid [5]. Regions of relatively high magnitude turbulence were associated with the upward-directed velocity within the central portion of the convecting cell, and regions of relatively low magnitude turbulence were associated with the downward-directed flow velocities near the sidewalls. These turbulence parameters are spatially-averaged in the x-direction at constant y/d, denoted by brackets $\langle\rangle$, and plotted as a function of distance from the grid, along with $\langle w_{rms} \rangle = \left\langle \sqrt{\overline{w'^2}} \right\rangle$ (Fig. 3). Here, two spatial averages are shown: centerline-values using $x/B = 0.45$–0.55, and entire-box values using $x/B = 0$–1.

In general, the distributions of turbulent velocities and kinetic energy agree qualitatively with previous work. All spatially-averaged turbulence parameters are maximized near, and decrease with distance from the grid. The rates of decay for the centerline values, however, differ from expected values (e.g., [18]), and the turbulent velocities do not decay with distance from the grid at the same rate. These differences are attributed to the current experimental

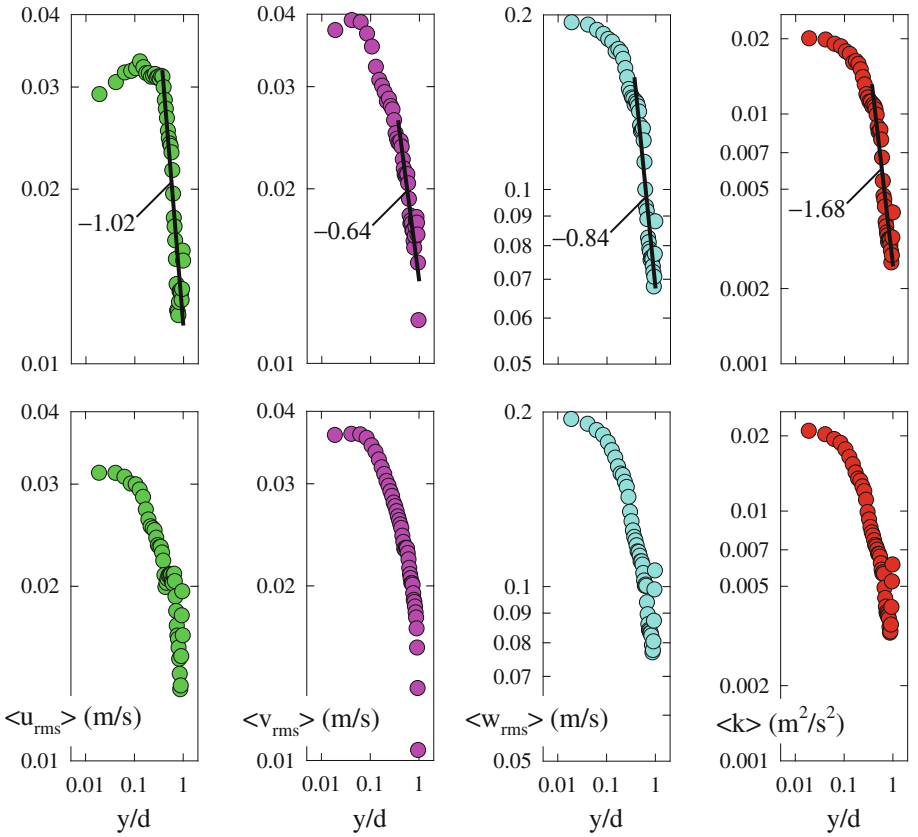

Fig. 3 Spatially-averaged root-mean-square velocities and turbulent kinetic energy values plotted as a function of distance away from the oscillating grid for the clear water condition using $f = 2.33$ Hz. The spatial averages are for $x/B = 0.45$–0.55 (*upper plots*; decay rates are given) and $x/B = 0$–1 (*lower plots*)

setup. In addition, three important observations are noted. First, there is a region of constant or slowly-decaying turbulence just above the grid, which extends a finite distance into the overlying flow. This can be interpreted as a region of developing turbulent flow, also referred to as the steady flow field [38]. For the centerline-values, this region of developing flow extends to $y/d \approx 0.37$, which corresponds to a distance approximately equal to S or $2M$, also noted by Thompson and Turner [38]. Second, there is a slight increase in turbulent velocities and kinetic energy near the water surface, consistent with water-surface interactions and upwelling and downwelling flow associated with the secondary circulation. Third, $\langle w_{rms} \rangle$ tends to be about five times larger than $\langle u_{rms} \rangle$ and $\langle v_{rms} \rangle$. As such, $\langle w_{rms} \rangle$ tends to dominate the contribution to $\langle k \rangle$ in these experiments. Consideration of just two velocity components (u and v), however, does not alter the results presented below.

3.2 Distributions of suspended sediment

Measurements of suspended sediment concentration within the mixing box were collected for a subset of the experiments. Using an input mass concentration of 1,000 g ($C_0 = 0.0130$) and an oscillation frequency of 2.33 Hz, vertical profiles of centerline suspended sediment

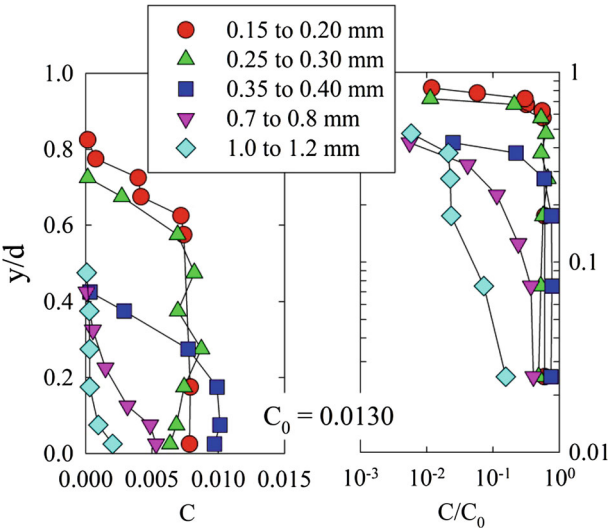

Fig. 4 *Vertical* variation in volumetric suspended sediment concentration C for different grain sizes measured at-a-point along the centerline the using $f = 2.33$ Hz

Table 1 For the suspended sediment profiles, the relative height y/d where concentration C tends to zero and where the inflection point in C occurs, as a function of grain size

Grain size range (mm)	y/d where $C \to 0$	y/d at inflection point in C
0.15–0.20	0.83	0.63
0.25–0.30	0.73	0.58
0.35–0.40	0.43	0.20
0.70–0.80	0.43	0.08
1.0–1.2	0.48	NA

NA means not applicable

concentration for the five grain sizes are shown in Fig. 4. In a companion study, Bennett et al. [5], monitored at-a-point suspended sediment concentration at three positions y/d above the grid using $f = 2.33$ Hz and $D = 0.25$ to 0.30 mm for a range of input suspended sediment concentrations ($C_0 = 0.0013$ to 0.0130). It was observed that at-a-point suspended sediment concentrations became nearly invariant when $C_0 > 0.0078$, and that this was accompanied by the observation of significant amounts of sediment remaining on the floor of the mixing box. This threshold concentration was interpreted to coincide with the transition from supply-limited conditions to transport-limited conditions, and that, above this concentration, steady-state suspended sediment conditions were attained. For all the suspended sediment data reported here, $C_0 = 0.0130$ and sediment was observed on the floor of the mixing box. Based on these observations, it is assumed that the sediment in suspension achieved steady-state conditions and the turbulent flow is not limited by sediment supply.

For a given input sediment mass, volumetric suspended sediment concentration and the maximum height attained within the flow are inversely proportional to grain size. Suspended sediment concentration tends to increase as grain size decreases, and suspended sediment occurs much higher in the flow field (farther away from the grid) for the smallest grain sizes (Fig. 4). The relative height above the grid where suspended sediment concentration tends to zero decreases as grain size increases (Table 1). While these data are limited in scope, this

result is to be expected because turbulence decays at a linear rate from the grid (Fig. 3), and distributions of suspended sediment reflect this vertical gradient. It is noted, however, that the concentration profiles also vary in shape. For the relatively fine grain sizes, the vertical profiles show nearly invariant concentrations of sediment to a critical height above the grid, then decrease gradually toward the water surface above this position, displaying a convex-upwards profile. For the relatively coarse grain sizes, this effect is diminished but still present. The relative height above the grid where this transition occurs (from nearly invariant to a convex-upwards suspended sediment concentration profile) also decreases as grain size increases (Table 1). Such a break does not appear to occur for $D = 1.0$–1.2 mm. Bennett and Best [3] observed similar results in their mixing box experiments. They employed a nearly identical facility and reported the vertical variation in suspended sediment flux for three quartz-density sediments (0.075–0.095, 0.18–0.21, and 0.30–0.36 mm) and for four different oscillation frequencies (1.1–3.4 Hz) as deduced by phase Doppler anemometry. While the input mass loadings employed were less than those reported here, the vertical profiles of suspended sediment flux for the finer grain sizes and higher frequencies (2.7 and 3.4 Hz) clearly displayed convex-upwards variations, whereas the coarsest sediment displayed concave-upwards vertical profiles for these frequencies. Moreover, Bennett and Best [3] also observed that the height attained within the flow by the sediment was proportional to the oscillation frequency and inversely proportional to grain size, consistent with the results presented here.

3.3 The effect of suspended sediment on secondary flow and the distribution of turbulent kinetic energy

The presence of suspended sediment has a marked effect on the secondary flow within the mixing box. Select examples of the secondary flow field within the mixing box are shown in Fig. 5. The flow field using $D = 0.25$–0.30 mm and $C_0 = 0.0013$ is qualitatively equivalent to the clear-water conditions shown in Fig. 2. As input sediment mass load increases, especially for the finer-grained sediment, there is a fundamental change in the secondary flow pattern. This additional mass, with its higher suspended sediment concentrations, causes the convection cells noted above to be all but obliterated, and the upward-directed secondary flow velocities to decrease in magnitude significantly, reversing entirely in direction at select locations (see Fig. 5b, d, f).

The alteration of the secondary flow depends on the amount of sediment in suspension. For $D < 0.4$ mm, all secondary flows are affected significantly for mass loadings of 700 g ($C_0 > 0.0091$) and higher, which results in relatively high suspended sediment concentrations, with observable effects occurring at loads as low as 400 g ($C_0 = 0.0052$). For $D > 0.7$ mm, however, the input sediment mass loads have little to no effect on the secondary flow field, presumably because little to no sediment is suspended, although some minor reduction in the magnitude of the upward-directed flow velocities is noted near the water surface.

The presence of suspended sediment also markedly affects the magnitude and distribution of turbulent kinetic energy. Contour plots of k for $D = 0.15$–0.25 mm for a range of sediment input concentrations C_0 are shown in Fig. 6. At relatively low concentrations ($C_0 < 0.006$), the magnitude and distribution of k within the measurement plane remain relatively unchanged. At progressively higher concentrations ($C_0 > 0.006$), the magnitude of k decreases significantly. In general, similar results are obtained for the turbulent components of velocity as well as for the finer grain sizes ($D < 0.40$ mm, with progressively smaller changes to the turbulence magnitude as grain size increases; not shown here).

It is contended here that the presence of significant suspended sediment alters the secondary flow circulation pattern within the mixing box. It is assumed that flow near the

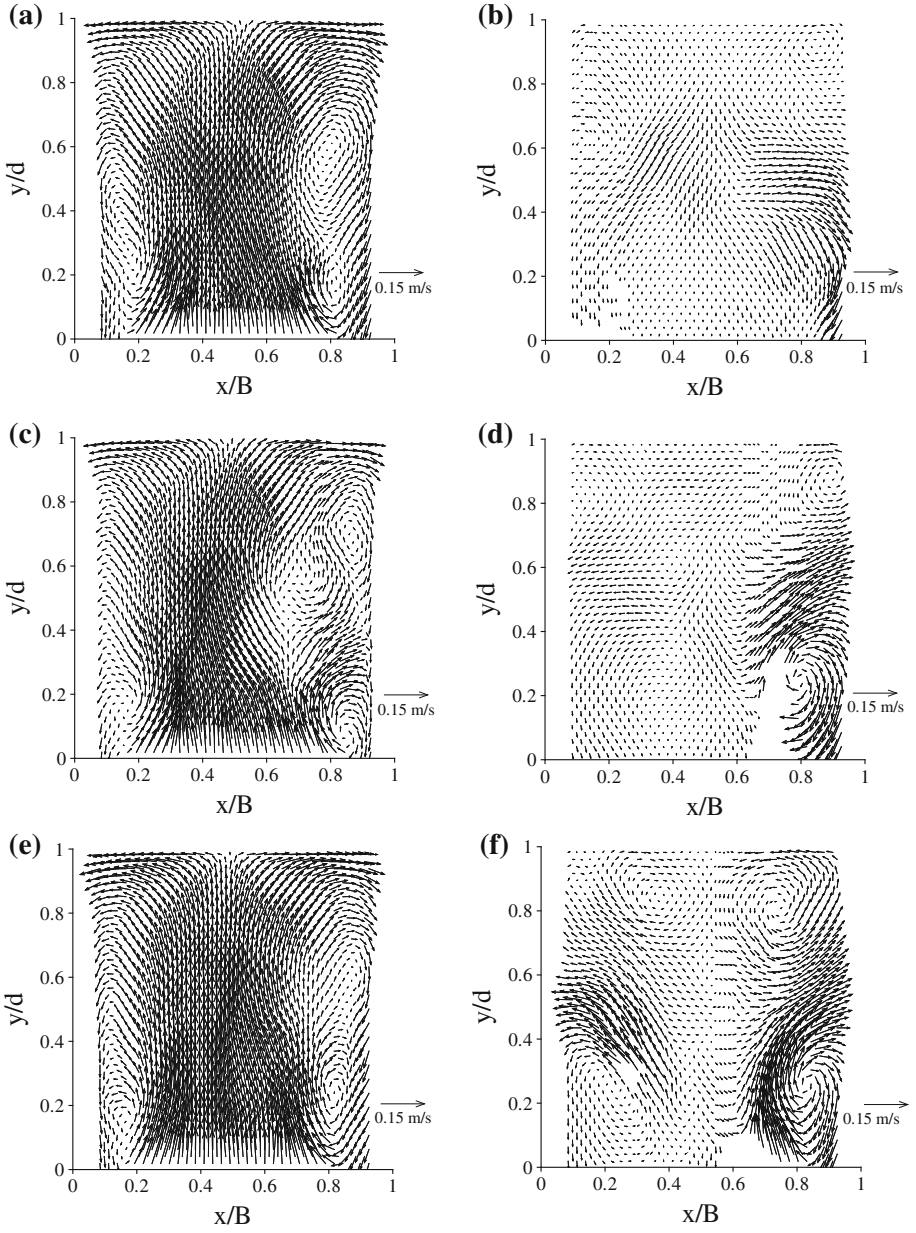

Fig. 5 Time-averaged 2D flow vectors within the mixing box using $f = 2.33$ Hz for $D = 0.15$–0.20 mm with **a** $C_0 = 0.0013$ and **b** $C_0 = 0.0130$, for $D = 0.25$–0.30 mm with **c** $C_0 = 0.0013$ and **d** $C_0 = 0.0130$, and for $D = 0.35$–0.40 mm with (e) $C_0 = 0.0013$ and **f** $C_0 = 0.0130$. Note that only one-half of vectors are shown here

sidewalls is predominantly directed downward in clear-water conditions. By increasing the suspended sediment load within the box, the relative thickness of the near-wall downward circulation increases, eventually intersecting the laser sheet at very high concentrations. In addition, the upward directed flows are displaced toward the center of the box. No such secondary

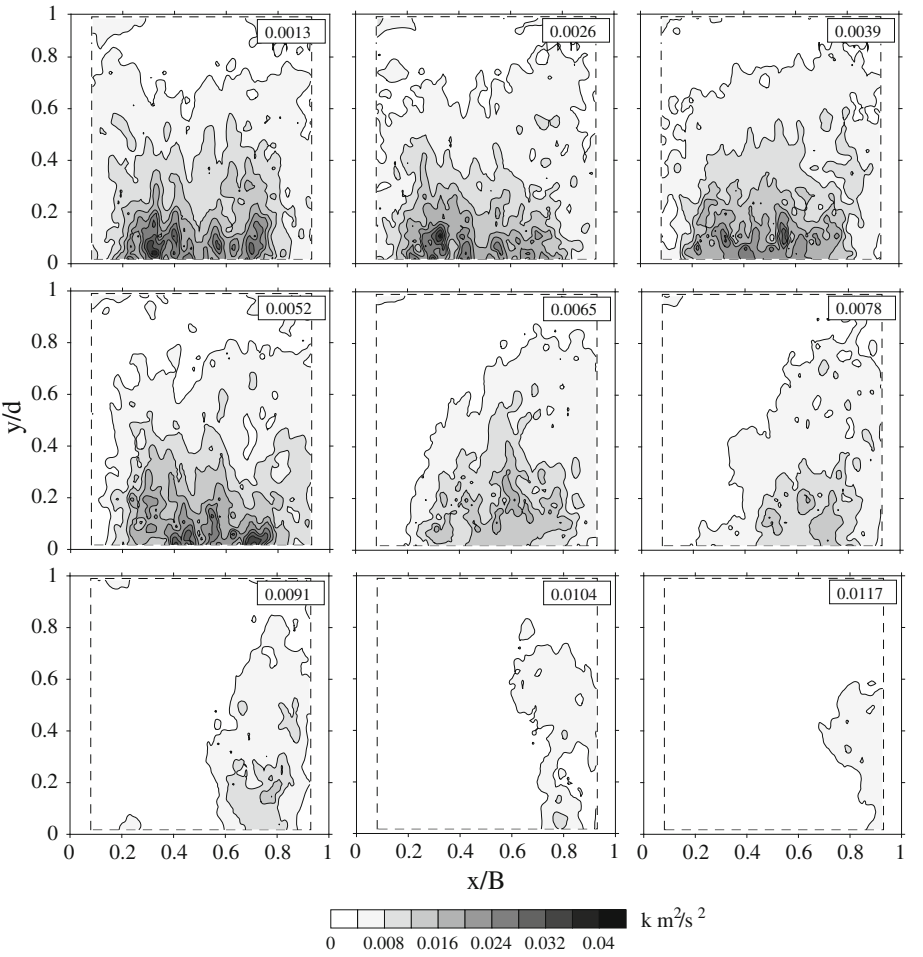

Fig. 6 Contour plots of time-averaged turbulent kinetic energy k within the mixing box using $f = 2.33$ Hz for $D = 0.15$–0.20 mm and for a range of input suspended sediment concentrations (from $C_0 = 0.0013$ to $C_0 = 0.0117$, as noted). The *dashed lines* represent the area where data were collected

flow modification is observed when coarser-grained sediment is introduced because the suspended sediment concentrations in the box for these grain sizes are insufficient to affect the flow. Therefore, the presence of significant sediment in suspension, with $C > 0.006$ at-a-point (see Fig. 4), is required to alter the secondary flow field using $f = 2.33$ Hz, and that this effect is accompanied by a marked reduction in turbulent kinetic energy (see Fig. 6 and below). The presence of sediment at the bottom of the box, potentially moving as bedload or as intermittently suspended material for the coarser grain-size experiments, does not affect the secondary flow field above the oscillating grid.

3.4 The effect of suspended sediment on horizontally-averaged turbulence

The presence of suspended sediment also has a significant impact on horizontally-averaged turbulence. Vertical profiles of spatially-averaged turbulent kinetic energy $\langle k \rangle$ are plotted as a function of relative height above the grid y/d for all experiments (Fig. 7). Included in these

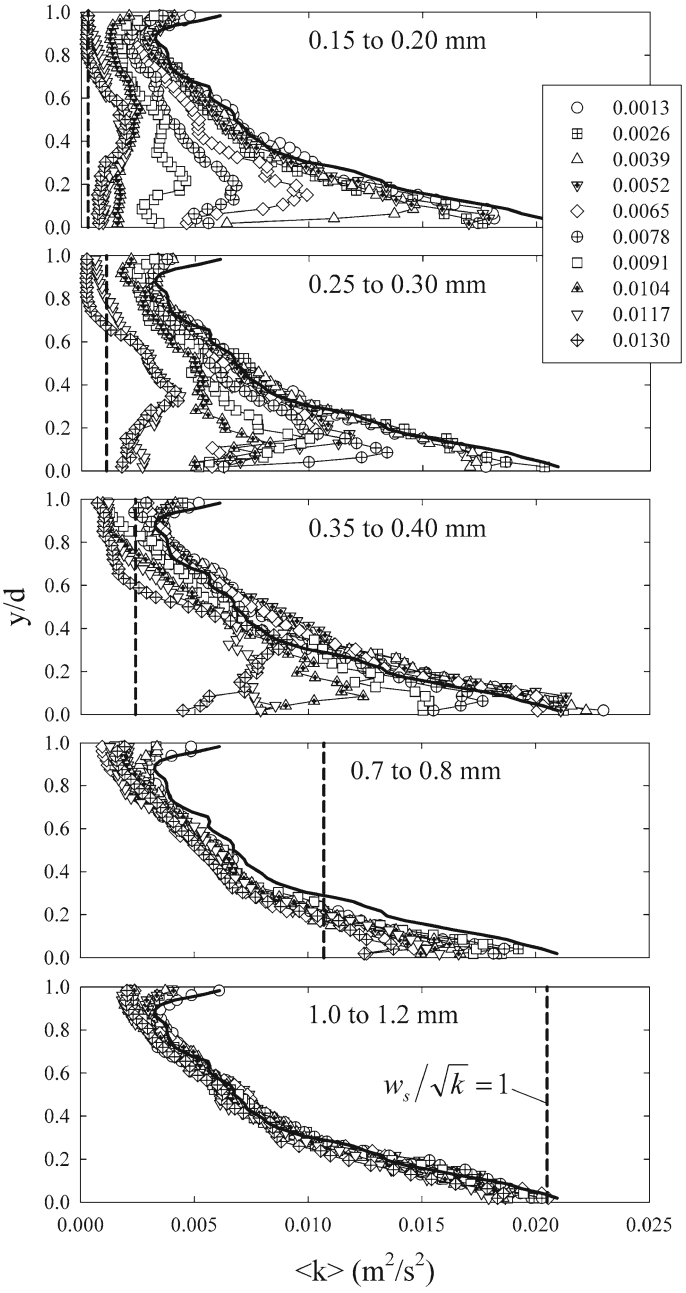

Fig. 7 Horizontally-averaged turbulent kinetic energy $\langle k \rangle$ as a function of relative distance away from the oscillating grid y/d with different input concentrations C_0 and sizes of sediment using $f = 2.33$ Hz. The *solid line* represents the clear-water condition and the *dashed line* represents the suspension criterion

plots are the values of $\langle k \rangle$ derived under clear-water conditions and a simple suspension criterion proposed by Michallet and Mory [29], defined as $w_s/\sqrt{k} = 1$ where w_s is the grain's settling velocity (determined here for spheres using Dietrich [9]). When $w_s/\sqrt{k} < 1$,

the sediment is assumed to be in suspension (to the right of the vertical line shown in Fig. 7). This suspension criterion is very similar to that employed in open channel flows (e.g., [4]), and it is wholly applicable to sediment-laden flows within mixing boxes.

In general, high concentrations of suspended sediment reduce the magnitudes of spatially-averaged turbulent kinetic energy. For the finer grain sizes ($D < 0.4$ mm), minor amounts of sediment mass loadings (<300 g or $C_0 < 0.0039$) do not cause any appreciable change in $\langle k \rangle$ as compared to the clear-water conditions (Fig. 7). When sediment mass loading reaches a critical level, $\langle k \rangle$ is reduced, most noticeably in the near-grid regions. This critical mass loading is 500 g ($C_0 = 0.0065$) for $D < 0.35$ mm, whereas it is 800 g ($C_0 = 0.0104$) for $D = 0.35$–0.40 mm. These results are consistent with the observed changes in the secondary flow field noted above. Moreover, at the highest sediment mass loadings for the finest grain sizes ($D < 0.3$ mm), corresponding to the highest suspended sediment concentrations within the box, the vertical gradient of $\langle k \rangle$ decreases significantly, attaining virtually no gradient for $D = 0.15$–0.20 mm for 1,000 g ($C_0 = 0.0130$; Fig. 7).

For the relatively coarser grain sizes ($D > 0.7$ mm), there is very little change in the magnitude of $\langle k \rangle$ as compared to the clear-water condition for all sediment loadings. Little alteration of the secondary flow field occurs for these grain sizes for all sediment loadings employed, and this lack of change is reflected in the vertical profiles of $\langle k \rangle$ (Fig. 7). The slight difference in $\langle k \rangle$ observed for $D = 0.7$–0.8 mm as compared to the clear-water condition is attributed to experimental variability.

The existence of suspended sediment and the reaction within the flow are consistent with the suspension criterion employed. For the finer grain sizes ($D < 0.4$ mm), the sediment can be suspended to relatively far distances above the grid, thus markedly affecting the secondary flow field and fluid turbulence. For the coarser grain sizes ($D > 0.7$ mm), little to no sediment suspension can occur, and little to no change in the flow field is observed. Moreover, the relative heights where $w_s/\sqrt{k} = 1$ agree reasonably well with the direct observations for the finer grain sizes ($D < 0.4$ mm) where $C \to 0$ for $C_0 = 0.0130$ as noted above (see Figs. 4, 7; Table 1). The largest discrepancies between the suspension criterion and the direct observations occur for the coarser grain sizes ($D > 0.7$ mm). Such discrepancy could be the result of sampling suspended sediment in the center of the box where k is at its maximum, and comparing this to the relatively lower, spatially-averaged values of $\langle k \rangle$ as used in Fig. 7.

3.5 The effect of suspended sediment on spatially-averaged turbulence, secondary flow, and total kinetic energy

The reaction of secondary and turbulent flow to suspended sediment also has a striking impact on spatially-averaged turbulence velocities, the magnitude of secondary flow velocity, and turbulent kinetic energy. To explore these effects, all data are spatially-averaged both vertically (y-direction) and horizontally (x-direction) to obtain a single, box-averaged value, designated by the double brackets $\langle\langle\rangle\rangle$. In addition, the magnitude of the secondary flow velocity U is determined at-a-point using

$$U = \sqrt{\bar{u}^2 + \bar{v}^2 + \bar{w}^2} \tag{3}$$

which also is vertically- and horizontally-averaged. Finally, all box-averaged values are normalized by the values obtained at the lowest input sediment loading ($C_0 = 0.0013$). Figure 8 plots these normalized, spatially-averaged values as a function of input sediment loading and grain size, e.g. $\langle\langle u_{rms} \rangle\rangle^* = \langle\langle u_{rms} \rangle\rangle / \langle\langle u_{rms} \rangle\rangle_{100}$, where the subscript 100 denotes the value obtained using an input mass loading of 100 g (or $C_0 = 0.0013$).

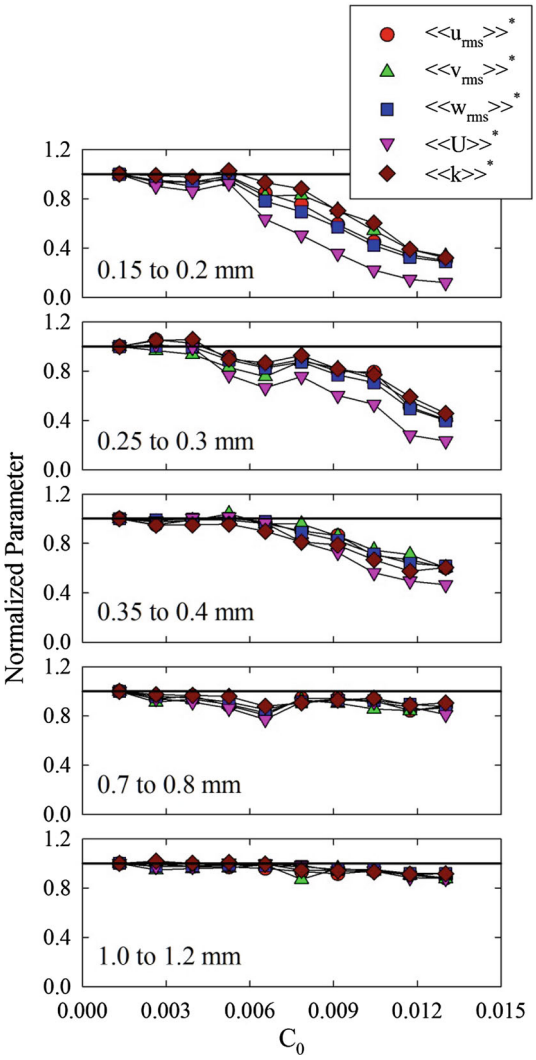

Fig. 8 Normalized spatially-averaged turbulent flow velocities, secondary flow velocity magnitude, and turbulent kinetic energy within the box as a function of input sediment concentration and grain size. All parameters are divided by the value observed at the lowest sediment load (100 g or $C_0 = 0.0013$). The *solid line* represents unity

The effect of suspended sediment on these spatially-averaged values increases in magnitude as the sediment size decreases and as input mass loading increases. For the finer grain sizes ($D < 0.4$ mm), markedly lower normalized turbulent velocities and turbulent kinetic energy (up to 80 % lower) and lower magnitudes of secondary flow velocity (up to 90 % lower) are observed (Fig. 8). These reductions are most pronounced at relatively high input sediment loads ($C_0 > 0.006$) and for the finer grain sizes. For the coarser grain sizes ($D > 0.7$ mm), the effect of input sediment load on the spatially-averaged values is minimized, yet there still exists a slight but observable reduction at higher sediment loads (up to 15 % reduction).

This reaction of the flow to suspended sediment can be extended to total kinetic energy. The total spatially-averaged kinetic energy $\langle\langle K\rangle\rangle$ can be defined as

$$\langle\langle K\rangle\rangle = \langle\langle k\rangle\rangle + 0.5\,\langle\langle U\rangle\rangle^2 \tag{4}$$

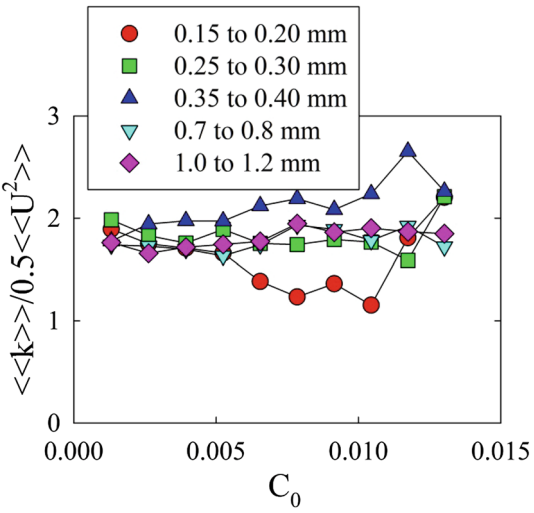

Fig. 9 The balance of spatially-averaged turbulent-to-mean kinetic energy within the box as a function of input sediment concentration and grain size

Figure 9 plots the spatially-averaged turbulent-to-mean kinetic energy ratio as a function of grain size and input sediment load. Based on these values, $\langle\langle k\rangle\rangle$ is about two times larger than $0.5\,\langle U\rangle^2$, and this ratio remains fairly constant for a range of grain sizes and input sediment loads. For all grains except $D = 0.35$–0.40 mm, the parameter $\langle\langle k\rangle\rangle/0.5\,\langle\langle U\rangle\rangle^2$ shows no statistically significant variation with increasing C_0. Yet for $D = 0.35$–0.40 mm, $\langle\langle k\rangle\rangle/0.5\,\langle\langle U\rangle\rangle^2$ does increase with increasing C_0 (statistically significant), suggesting that $\langle U\rangle^2$ decreases at a faster rate than $\langle\langle k\rangle\rangle$. Since this ratio, in general, remains relatively constant for most of the experimental conditions, suspended sediment appears to reduce both the turbulent and mean kinetic energy equally within the flow (see [30]).

3.6 The effect of suspended sediment on integral time and length scales

Integral time and length scales for the larger eddies within the flow can be determined as a function of suspended sediment concentration. The integral time scale of a turbulent flow refers to the characteristic scale of the larger eddies, which can be calculated through autocorrelation analysis [34,37]. The autocorrelation coefficient $R_{ii}\,(\Delta t)$ for the fluctuating cross-stream velocity component u', for example, over time t at a given location x and y is defined as

$$R_{ii}\,(\Delta t) = \frac{\overline{u'\,(x,\,y,\,t)\,u'\,(x,\,y,\,t+\Delta t)}}{\overline{u'\,(x,\,y)^2}} \tag{5}$$

where Δt is the time lag over which the autocorrelation is calculated and the overbar signifies a temporal average. The integral time scale then is determined from

$$\tau = \int_0^\infty R_{ii}\,(\Delta t)\,\mathrm{d}\,(\Delta t) \tag{6}$$

The upper limit of the integration is set by the number of time intervals or the length of data recorded, and it usually coincides with the first zero-crossing of the $R_{ii}\,(\Delta t)$ values. The integral length scale λ then can be calculated by multiplying the integral time scale τ by a characteristic velocity at that same location. Here, the root-mean-square velocity is used

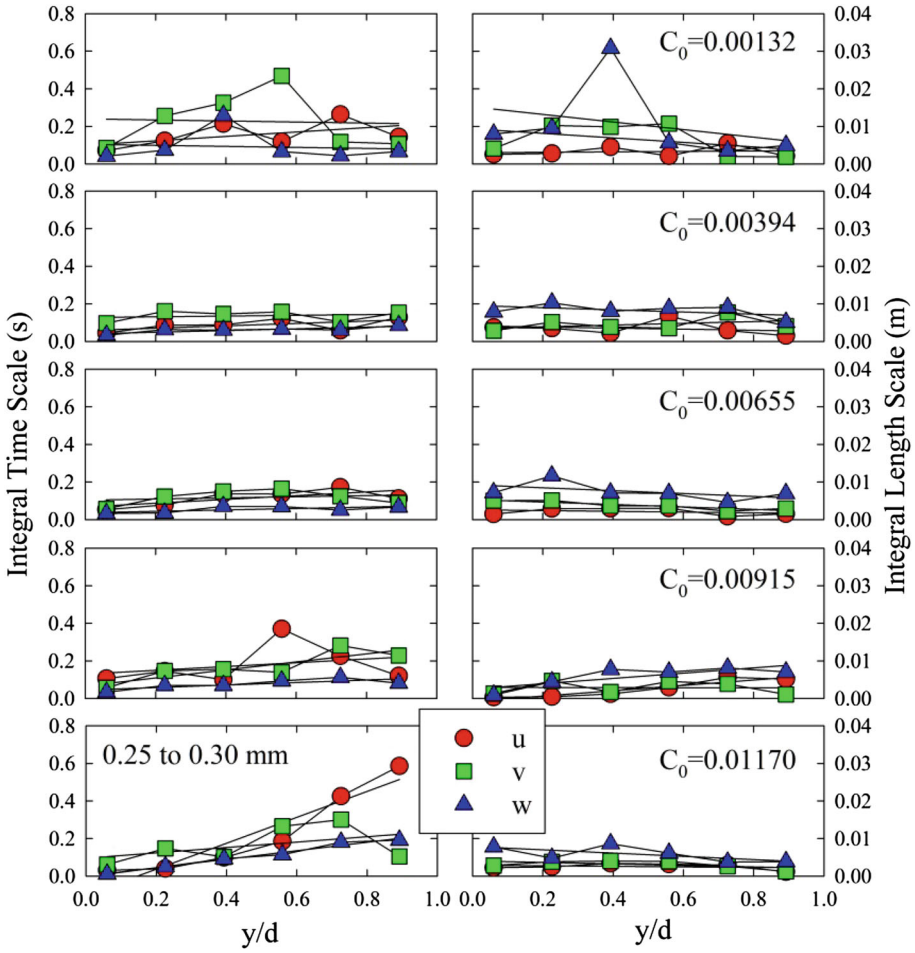

Fig. 10 An example plot of the *vertical* variation of integral time (on *left*) and length (on *right*) scales for each velocity component for the 0.25–0.30 mm sediment. Five different input sediment concentrations (C_0) are shown, along with *least-squares* linear regression *lines* for each velocity component

([10]; using the absolute value of the time-averaged velocity instead has no effect on the trends reported below).

Autocorrelation analysis is applied to all sediment-laden conditions at discrete positions within the box. Two vertical profiles (an off-axis location at $x/B = 0.20$ and a centerline location at $x/B = 0.51$), each with six positions above the grid ($y/d = 0.06$, 0.23, 0.39, 0.56, 0.73, and 0.89), are selected for analysis. At each location, values of τ and λ are derived for all grain sizes, sediment concentrations, and velocity components. These data then are plotted as a function of height above the grid and grouped by input sediment concentration, and as a function of input sediment concentration and grouped by location. Examples of these plots are shown in Figs. 9 and 10, respectively. In general, τ varies from 0.1 to 0.4 s, which is very close to the oscillation period of the grid (0.43 s), and λ varies from 0.005 to 0.02 m, which is very close to the bar thickness (0.01 m) and mesh size (0.04 m) of the grid (see [10]). These observations support the precept that the autocorrelation analysis quantifies the

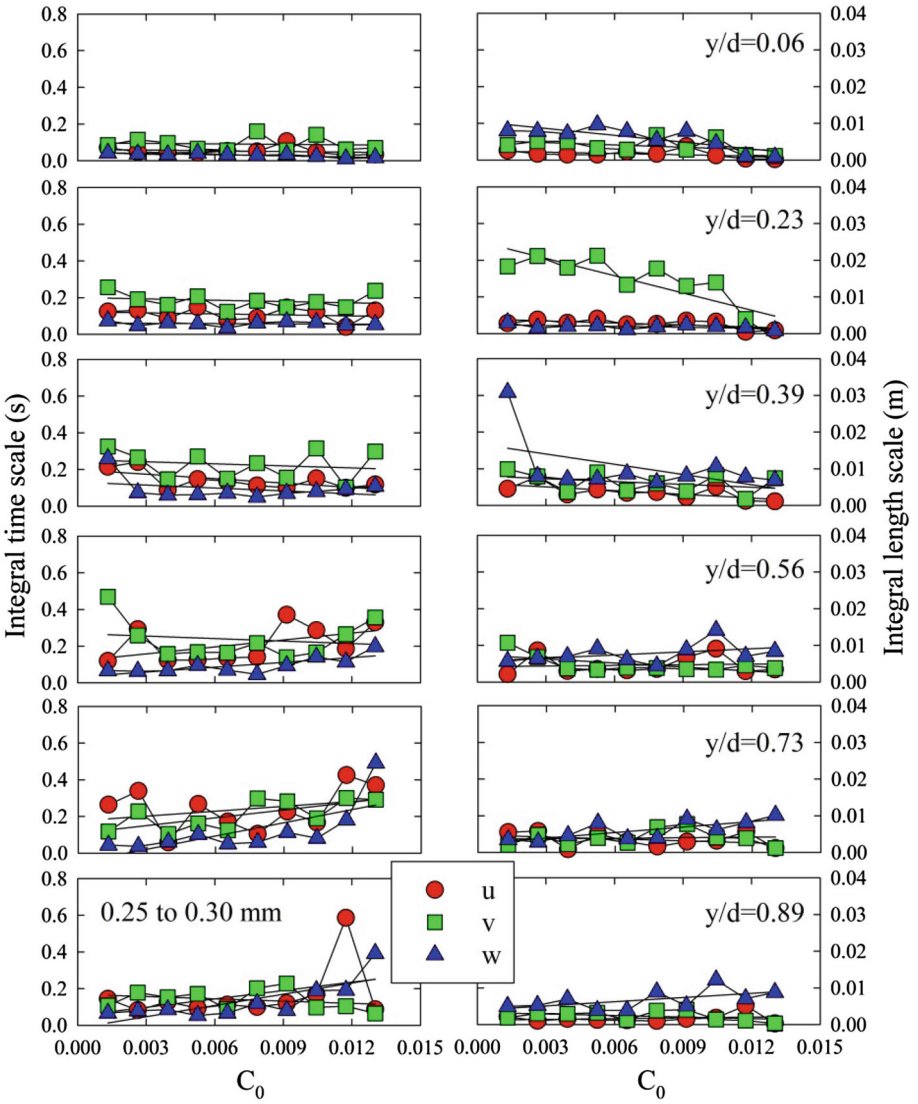

Fig. 11 An example plot of the variation of integral time (on *left*) and length (on *right*) scales for each velocity component as a function of input sediment concentrations (C_0) for the 0.25–0.30 mm sediment. Six different heights above the grid along the mixing box's centerline are shown, along with *least-squares* linear regression *lines* for each velocity component

characteristic scales of the larger eddies, which should be strongly related to the oscillation frequency and dimensions of the grid. By assuming that $\lambda \approx 0.01$ m and using v_{rms} in Eq. (1), Stokes numbers St for each grain size can be approximated as follows: 10^{-3}–10^{-2} for $D < 0.40$, 10^{-2} for $D = 0.35$–0.40 mm, and 10^{-1} for $D > 0.7$.

Statistical analyses are performed on the derived time and length scales to determine if these values are altered by the presence of suspended sediment. This analysis seeks to examine if these integral scales change with height above the grid for a given input sediment load (e.g., Fig. 10), and input sediment load at a given location above the grid (e.g., Fig. 11). Table 2

Table 2 Ensemble results of autocorrelation analysis and the derivation of integral time and length scales for all experiments

Grain size (mm)	Effect of height				Effect of concentration			
	Centerline		Off-axis		Centerline		Off-axis	
	Statistically significant trends[a] (%)	Positive trends (%)	Statistically significant trends (%)	Positive trends (%)	Statistically significant trends (%)	Positive trends (%)	Statistically significant trends (%)	Positive trends (%)
Integral time scale								
0.15–0.20	40	92	50	93	33	17	17	100
0.25–0.30	33	100	40	100	28	80	44	88
0.35–0.4	40	100	60	100	22	100	33	83
0.7–0.8	53	94	60	100	22	75	6	0
1.0–1.2	50	93	53	94	11	50	6	0
Integral length scale								
0.15–0.20	33	40	23	29	44	0	28	0
0.25–0.30	23	43	23	43	22	25	17	0
0.35–0.4	30	22	37	73	0	NA	11	0
0.7–0.8	37	36	10	67	6	0	0	NA
1.0–1.2	30	11	17	60	6	100	0	NA

Only the percentage of statistically significant trends and the percentage of those trends that are positive (those that increase in magnitude with distance or concentration) are reported as a function of increasing height above the grid and sediment concentration at two positions within the mixing box (centerline and off-axis)

[a] Trends are considered statistically-significant when the correlation coefficient of the regression line is equal to or greater than 0.4

summarizes the ensemble results for the experiments. For all sediment input concentrations, integral time scale increases with distance above the grid in about 50 % of the experiments using all velocity components and all grain sizes, whereas integral length scale does not show any clear trend of statistical significance. For this latter variable, only about 30 % of the experiments display a statistically significant trend, and most of these are negatively correlated with distance above the grid. For both integral time and length scales, an increase in input sediment concentration does not affect these values significantly at-a-point above the oscillating grid for all velocity components and for all grain sizes examined. Based on these data, τ and λ show no systematic variation within the zero mean-shear flow in response to the addition of sediment and the presence of a suspended load for any sediment size considered.

4 Discussion

Fluid turbulence within the zero mean-shear flow is markedly altered by the presence of suspended sediment. In all cases, turbulent kinetic energy decreases significantly as the volumetric suspended sediment concentration increases. This means that for a given oscillation frequency, turbulent suppression also increases as grain size decreases. These results are the clearest experimental evidence for the suppression of turbulence by suspended sediment yet obtained. While a number of mechanisms have been proposed to explain the modulation of fluid turbulence by the presence of quartz-density suspended sediment, most numerical models of two-phase flows assume that energy transferred from turbulence to particles is dissipated rapidly, and this increased dissipation rate leads to turbulence suppression [2]. The results presented herein, however, may not support this hypothesis (see below).

Time and length scales do not display any systematic variation with suspended sediment load within the flow. Autocorrelation analysis also demonstrates no consistent statistical variation of τ and λ within the flow in response to suspended sediment concentrations for any grain size used. These observations have important implications for the proposed criteria for turbulence modulation. Integral time τ and length λ scales for grid-generated turbulence may be related to turbulent kinetic energy k and the rate of dissipation of this energy ε using ([34]; see also [27,29,32]):

$$\tau \equiv \frac{k}{\varepsilon}; \quad \lambda \equiv \frac{k^{3/2}}{\varepsilon} \tag{7}$$

Turbulent kinetic energy k_0 and the rate of dissipation of this energy ε_0 at the mid-point of the oscillating grid can be defined as simple functions of grid frequency f, stroke S, and mesh size M [29]. Values of k and ε at any height above the grid also have been shown to depend only on k_0, ε_0, and relative height y/d [27]. For the experiments herein, f, S, and M are constant, thus k_0 and ε_0 also should be constant, and k and ε should decrease with y/d. Since k decreases with increasing suspended sediment concentration (Figs. 6, 7, 8) while both τ and λ remain statistically unchanged (Figs. 10, 11), the rate of dissipation of turbulent energy ε must also decrease as suspended sediment concentration increases, if both Eq. (7) and the analytic formulations of Matsunaga et al. [27,29] are applicable to the present experiment. Li et al. [23] noted that the presence of suspended sediment in a simulated turbulent gas flow causes a reduction in k that is accompanied concomitantly by a reduction in ε. Thus it is suggested here that the reduction in k in the flow is due to the transfer of this energy to the sediment in suspension (e.g., [39]), rather than due to an increase in ε as previously suggested (e.g., [2,35]). This issue is further addressed below.

Criteria to discriminate the modulation of turbulence by suspended sediment based on integral time and length scales of turbulence cannot be employed to explain the observations reported here. Hou [19] used these data to critically assess the turbulence modulation criterion proposed by Gore and Crowe [14], i.e., fluid turbulence is enhanced when $D/\lambda > 0.1$ and suppressed when $D/\lambda < 0.1$. Hou [19] demonstrated that this criterion cannot be used here, since no correlation exists between D/λ and the observed changes in turbulent kinetic energy. Although the data do support the assertion made by Gore and Crowe [14], that turbulent energy of eddies is transformed into kinetic energy of particle motion, the actual turbulence modulation criterion as proposed cannot be supported (see also [24,36]). Moreover, the Stokes number criterion (Eq. 1) also cannot be used to explain the observations reported because the only parameter that appears to be sensitive to increasing suspended sediment concentration is turbulence. That is, as suspended sediment concentration increases, v_{rms} decreases while λ remains statistically constant, thus increasing t_f and decreasing St (t_p also remains constant). In both cases, the physical mechanism of turbulence modulation by suspended sediment is not captured by the suggested criteria.

Density stratification, however, can occur in zero mean-shear flows due to the presence of suspended sediment, and this could affect turbulence. Noh and Fernando [32] suggested that the existence of a horizontal front (lutocline), across which the diffusion of particles and turbulent energy are inhibited, can be identified by the shape of the vertical concentration profile and by the use of dimensionless expressions. First, when $-\partial C/\partial y$ within the sediment-laden flow decreases to zero monotonically, no front exists. Whereas when $-\partial C/\partial y$ first increases with y and then decreases rapidly to zero, a front exists, and the location of the inflection point $-\partial^2 C/\partial y^2 = 0$ can be used as the depth of the suspension layer. The suspended sediment profiles for the transport-limited conditions shown in Fig. 4 could support this stratification thesis, since clear inflection points (convex-upward profiles) are observed (see Table 1). Also, the vertical profiles of $\langle k \rangle$ for these grain sizes and an input mass loading of 1,000 g ($C_0 = 0.0113$) display nonlinearities near each of these critical y/d values (Fig. 7), suggesting the possible existence of a horizontal front. Second, Noh and Fernando [32] derived a dimensionless criterion for the existence of a front, based on the values for R^* and G^*, defined as

$$R^* = w_s/U^* \tag{8}$$

$$G^* = \frac{g\,(\sigma - \rho)}{\rho}\frac{LC^*}{U^{*2}} \tag{9}$$

where U^* is a characteristic velocity (defined as $U^* = k^{1/2}$ at $y/d \approx 0$), L is a characteristic length scale (defined as $L = \lambda$ at $y/d \approx 0$), C^* is a characteristic volumetric concentration (defined as $C^* = \int_0^\infty C dy$). Here, Eq. (8) represents the commonly used suspension criterion, and Eq. (9) represents a Richardson number commonly employed to characterize stratified flows. Given the empirical constants required for this derivation, Noh and Fernando [32] also defined $R = c_4 R^*$ and $G = c_5 G^*$, where $c_4, c_5 \approx 1$. For $R << 1$, ($R < 0.08$), no well-defined front forms when $G \leq 2.2R^2$, and both turbulence and suspended sediment concentration decrease systematically away from the grid. When $G > 2.2R^2$, a front appears and the diffusion of turbulent energy and suspended sediment therefore are inhibited. Figure 12 compares this dimensionless criterion to the data collected herein, using the appropriate values. Strict application of this criterion, however, suggests that no front would be present for any of the experimental conditions. If it is accepted that a front is present in select experiments, as suggested above, then the criterion could be modified to $G \sim 0.0022R^2$ (or by changing c_5; Fig. 12). Since k is modulated by C, a grid-specific value of k could have been employed,

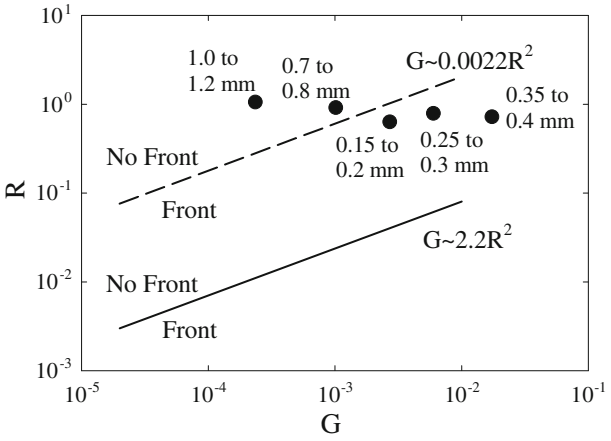

Fig. 12 Criterion for the formation of a *horizontal* front following [32] using the suspension criterion R and a Richardson number G, compared to the data presented herein

such as the one observed using the 1.0–1.2 mm sediment. While this grid-specific k would have been greater in magnitude for the finer sediment sizes, thus reducing both R and G, this substitution would not have altered significantly the results shown in Fig. 11. In summary, there is evidence to support the formation of a stratified layer within the mixing box for the finer grain sizes ($D < 0.7$ mm), based on the vertical profiles of suspended sediment concentration and turbulent kinetic energy and an analytic criterion for the existence of a horizontal front. Yet these results are not entirely conclusive.

Turbulence modulation by suspended sediment also markedly affects boundary layer characteristics. As noted above, the thickness of the sidewall boundary layer and secondary flow pattern within the box are altered, and both turbulent and mean kinetic energy are reduced as suspended sediment concentrations increase (Figs. 5, 6, 7, 8, 9). These modifications occur in spite of the continued oscillation of the grid.

Lastly, the upward diffusion of grid-generated turbulence should have the ability to maintain a suspended sediment load, as momentum is transferred from the fluid to the sediment. This idea was first postulated by Bagnold [1] in open channel flow, and the results presented herein already support this statement (e.g., Figs. 3 and 4; see [20]). Leeder et al. [22] further quantified this process by showing that an upward-directed momentum flux can be balanced by the immersed weight of suspended load over unit bed area, such that the maintenance of the suspended load occurs when this ratio is greater than one, or

$$\frac{\rho(\overline{v'^2})_{\max}}{m\,[(\sigma-\rho)/\sigma]\,g} > 1 \tag{10}$$

where the numerator is the maximum normal turbulent stress as expressed by the vertical velocity component (N/m^2) and m is the total sediment mass per unit bed area (kg/m^2). To apply this criterion, m represents the total mass per unit bed area above each position y/d, which is depth-integrated from this location to the height where $C \rightarrow 0$ (see Fig. 4 and Table 1), and $\langle k \rangle \approx \left(\overline{v'^2}\right)_{\max}$, which already has been shown to be an appropriate suspension criterion. Figure 13 demonstrates that this criterion works well for the data collected, suggesting that the suspended sediment load is maintained by this transfer of fluid momentum, or fluid-particle interactions. There also is a maximum value of $m\,[(\sigma-\rho)/\sigma]\,g \approx 10^1$ for

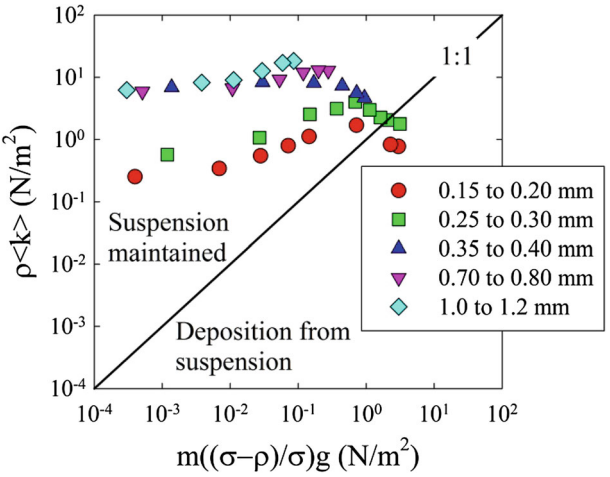

Fig. 13 Criterion for the maintenance of a suspended sediment load

the observations made, which makes theoretical sense since M, S, and f are constant (see Eq. 2). Finally, the suspension criterion appears to remain applicable even when turbulence is modulated by the presence of suspended sediment.

In summary, the suppression of fluid turbulence due to the presence of suspended sediment within a zero-mean shear flow appears to be the result of fluid-particle interactions. Fluid momentum must be transferred to the sediment so as to maintain the suspended load. Zhao et al. [39] suggested that this transfer of energy from the fluid to the particle, thus suspending the sediment, is not balanced by the transfer of energy from the particle to the fluid. As a result, there is a net loss of kinetic energy within the fluid, which can be considered a particle-induced energy dissipation. This energy loss could be accompanied by a reduction in the magnitude of the secondary flow within the mixing box and potentially the rate of turbulent energy dissipation as shown here (e.g., [23]). It is possible that density stratification within the flow due to the suspension of sediment could alter the upward diffusion of the fluid turbulence (e.g., [32]), but the experimental evidence in support of this physical mechanism is inconclusive. This coupled effect of potentially stratified flow, reduced turbulent energy, and altered boundary conditions and secondary flow field in response to suspended sediment concentrations may provide an alternate physical mechanism for turbulence modulation observed in geophysical flows, most notably sediment-laden open channels.

5 Conclusions

While much information on the modulation of fluid turbulence by suspended sediment exists, these effects in open channel flows can be varied and the exact mechanisms remain poorly understood. The current research sought to address specific limitations posed in the examination of sediment-laden geophysical flows in laboratory settings by employing PIV to discriminate the fluid phase unambiguously and by using a standard mixing box where the frequency of the oscillating grid, the size and concentration of the sediment placed into it, and the flow depth all can be controlled with great precision.

Using both clear-water and sediment-laden conditions, the following conclusions can be drawn from this experimental campaign.

1. For the experimental conditions, the oscillating grid creates a secondary flow pattern with a central domain dominated by upward-directed flow and bounded on either side by convection cells.
2. Turbulent velocities and kinetic energy are maximized near the grid, but there exists a region of developing flow that extends to $y/d \approx 0.37$ (approximately equal to S or $2M$) where the turbulence magnitudes do not vary. Above this height, these turbulence values decrease systematically toward the water surface.
3. Suspended sediment concentration and the maximum height attained by this sediment are inversely proportional to grain size. Convex-upwards vertical profiles of suspended sediment are observed for the finer grain sizes, which may be indicative of sediment stratification.
4. Relatively high concentrations of suspended sediment can significantly alter the secondary flow field and markedly reduce both the turbulent and spatially-averaged kinetic energy. Relatively coarser-grain sediment at the same mass loadings has no measurable effect on secondary flow and turbulence because little of this sediment can be suspended by the oscillating grid.
5. Derived integral time scales for all velocity components are similar to the oscillation frequency of the grid, and derived integral length scales are similar to the bar thickness and mesh size. Yet an increase in suspended sediment concentration or a change in height above the grid does not alter these values systematically or statistically.
6. The overall reduction in turbulent kinetic energy within the zero mean-shear flow can be related to the transfer of energy from the fluid to the sediment and the energy required to maintain this suspended sediment load. Turbulence modulation criteria based on the alteration of integral time and length scales cannot be used to explain the observations reported here.

The results obtained in a zero mean-shear flow demonstrate unequivocally that the suspension of quartz-density sediment and the maintenance of this suspended sediment load markedly reduce the turbulent and time-mean kinetic energy of the fluid. These results should be applicable to a range of sediment-laden geophysical flows in natural environments.

Acknowledgments We would like to thank Kevin Cullinan and Michael Fay for technical assistance with the experiments, Mike Leeder for helpful discussions on his suspension criterion, and the anonymous referees for suggesting ways to improve the clarity of the paper. This research was supported by NSF EAR 0549607.

References

1. Bagnold RA (1966), An approach to the sediment transport problem from general physics. U.S. Geological Survey Professional Paper 422-I, 37 pp
2. Balachandar S, Eaton JK (2010) Turbulent dispersed multiphase flow. Annu Rev Fluid Mech 42:111–133
3. Bennett SJ, Best JL (1995) Particle size and velocity discrimination in a sediment-laden turbulent flow using phase Doppler anemometry. J Fluids Eng 117:505–511
4. Bennett SJ, Bridge JS, Best JL (1998) Fluid and sediment dynamics of upper-stage plane beds. J Geophys Res 103(C1):1239–1274
5. Bennett SJ, Atkinson JF, Hou Y, Fay MJ (2013) Turbulence modulation by suspended sediment in a zero mean-shear geophysical flow. In: Venditti JG, Best J, Church M, Hardy RJ (eds) Coherent flow structures at the earth's surface. Wiley, Chichester, pp 309–321. doi:10.1002/9781118527221.ch20
6. Best J, Bennett S, Bridge JS, Leeder M (1997) Turbulence modulation and particle velocities over flat sand beds at low transport rates. J Hydraul Eng 123:1118–1129

7. Bridge JS, Bennett SJ (1992) A model for the entrainment and transport of sediment grains of mixed sizes, shapes and densities. Water Resour Res 28:337–363
8. De Silva IPD, Fernando HJS (1998) Experiments on collapsing turbulent regions in stratified fluids. J Fluid Mech 358:29–60
9. Dietrich WE (1982) Settling velocity of natural particles. Water Resour Res 18(6):1615–1626
10. Dohan K, Sutherland BR (2002) Turbulence time scales in mixing box experiments. Exp Fluids 33:709–719
11. Elghobashi S (1994) On predicting particle-laden turbulent flows. Appl Sci Res 52:309–329
12. Elghobashi S, Truesdell GC (1993) On the two-way interaction between homogeneous turbulence and dispersed solid particles. II: turbulence modification. Phys Fluids A 5(7):1790–1801
13. García MH (2008) Sediment transport and morphodynamics. In García MH (ed) Sedimentation engineering: processes, management, modeling, and practices. ASCE Manuals and Reports on Engineering Practice No. 110, American Society of Civil Engineers, Reston, VA, pp 21–163
14. Gore RA, Crowe CT (1989) Effect of particle size on modulating turbulent intensity. Int J Multiph Flow 15:279–285
15. Gore RA, Crowe CT (1991) Modulation of turbulence by a dispersed phase. J Fluids Eng 113:304–307
16. Hetsroni G (1989) Particle-turbulence interaction. Int J Multiph Flow 15:735–746
17. Hinze JO (1959) Turbulence. McGraw-Hill, New York
18. Hopfinger J, Toly JA (1976) Spatially decaying turbulence and its relation to mixing across density interfaces. J Fluid Mech 78:155–175
19. Hou Y (2011) Turbulence modulation by suspended sediment within a mixing box. MS thesis, University at Buffalo, Buffalo
20. Huppert HE, Turner JS, Hallworth MA (1995) Sedimentation and entrainment in dense layers of suspended particles stirred by an oscillating grid. J Fluid Mech 289:263–293
21. Kaftori D, Hetsroni G, Banerjee S (1995) Particle behavior in the turbulent boundary layer. I. Motion, deposition, and entrainment. Phys Fluids 7:1095–1106
22. Leeder MR, Gray TE, Alexander J (2005) Sediment suspension dynamics and a new criterion for the maintenance of turbulent suspensions. Sedimentology 52:683–691
23. Li Y, McLaughlin JB, Kontomaris K, Portela L (2001) Numerical simulation of particle-laden turbulent channel flow. Phys Fluids 13:2957–2967. doi:10.1063/1.1396846
24. Lucci F, Ferrante A, Elghobashi S (2011) Is Stokes number an appropriate indicator for turbulence modulation by particles of Taylor-length-scale size? Phys Fluids 23:025101
25. Lyn DA (1991) Resistance in flat-bed sediment-laden flows. J Hydraul Eng 117:94–114
26. Lyn DA (1992) Turbulence characteristics of sediment-laden flows in open-channels. J Hydraul Eng 118:971–988
27. Matsunaga N, Sugihara Y, Komatsu T, Masuda A (1999) Quantitative properties of oscillating-grid turbulence in a homogeneous fluid. Fluid Dyn Res 25:147–165
28. McKenna SP, McGillis WR (2004) Observations of flow repeatability and secondary circulation in an oscillating grid-stirred tank. Phys Fluids 16:3499–3502
29. Michallet H, Mory M (2004) Modelling of sediment suspensions in oscillating grid turbulence. Fluid Dyn Res 35:87–106
30. Muste M, Yu K, Fujita I, Ettema R (2005) Two-phase versus mixed-flow perspective on suspended sediment transport in turbulent channel flows. Water Resour Res 41:W10402. doi:10.1029/2004WR003595
31. Nezu I, Azuma R (2004) Turbulence characteristics and interaction between particles and fluid in particle-laden open channel flows. J Hydraul Eng 130:988–1001
32. Noh Y, Fernando HJS (1991) Dispersion of suspended particles in turbulent flow. Phys Fluids A 3:1730–1740
33. Orlins JJ, Gulliver JS (2003) Turbulence quantification and sediment resuspension in an oscillating grid chamber. Exp Fluids 34:662–677
34. Pope SB (2000) Turbulent flows. Cambridge University Press, New York
35. Schreck S, Kleis SJ (1993) Modification of grid-generated turbulence by solid particles. J Fluid Mech 249:665–688
36. Tanaka T, Eaton JK (2008) Classification of turbulence modification by dispersed spheres using a novel dimensionless number. Phys Rev Lett 101:114502
37. Tennekes H, Lumley JL (1972) A first course in turbulence. The MIT Press, Cambridge
38. Thompson SM, Turner JS (1975) Mixing across an interface due to turbulence generated by an oscillating grid. J Fluid Mech 67:349–368
39. Zhao L, Andersson HI, Gillissen JJJ (2013) Interphasial energy transfer and particle dissipation in particle-laden wall turbulence. J Fluid Mech 715:32–59